RAPID RESEARCH LETTER

physica
status
solidi **rrl**
www.pss-rapid.con

Check for updates

Effect of Dopant Ordering on the Stability of Ferroelectric Hafnia

Sangita Dutta, Hugo Aramberri, Tony Schenk, and Jorge Íñiguez*

Films of the all-important compound hafnia (HfO₂) can be prepared in an orthorhombic ferroelectric (FE) state that is ideal for applications, e.g., in memories or negative-capacitance field-effect transistors. The origin of this FE state remains a mystery, though, as none of the proposed mechanisms for its stabilization—from surface and size effects to formation kinetics—is fully convincing. Interestingly, it is known that doping HfO₂ with various cations favors the occurrence of the FE polymorph; however, existing first-principles works suggest that doping by itself is not sufficient to stabilize the polar phase over the usual nonpolar monoclinic ground state. Herein, first-principles methods are used to re-examine this question. Two representative isovalent substitutional dopants, Si and Zr, are considered, and their preferred arrangement within the HfO₂ lattice is studied. The results reveal that small atoms like Si can adopt very stable configurations (forming layers within specific crystallographic planes) in the FE orthorhombic phase of HfO₂ but comparatively less so in the nonpolar monoclinic one. Further, it is found that, at low concentrations, such a dopant ordering yields a FE ground state, the usual paraelectric phase becoming a higher-energy metastable polymorph. The implications of the findings are discussed.

Ever since it was shown that HfO₂ films can be prepared in a ferroelectric (FE) phase,[1,2] much effort has focused on elucidating the origin of such a surprising state, never observed in bulk form. Ferroelectricity in hafnia generally becomes more robust as the size of the grains or crystallites gets smaller,[3] a feature that is just opposed to what is typical in traditional FEs (e.g., perovskite oxides) and seems to suggest that surface effects play a role in the stabilization of the polar polymorph.[4]

S. Dutta, Dr. H. Aramberri, Dr. T. Schenk, Prof. J. Íñiguez
Materials Research and Technology Department
Luxembourg Institute of Science and Technology (LIST)
Avenue des Hauts-Fourneaux 5, L-4362 Esch/Alzette, Luxembourg
E-mail: jorge.iniguez@list.lu

S. Dutta, Prof. J. Íñiguez
Department of Physics and Materials Science
University of Luxembourg
Rue du Brill 41, L-4422 Belvaux, Luxembourg

The ORCID identification number(s) for the author(s) of this article can be found under https://doi.org/10.1002/pssr.202000047.

However, evidence for this explanation is not conclusive and, more recently, other possible factors, ranging from kinetics of formation of the FE phase to the role of phase boundaries and local strains, have been discussed.[5–10]

Interestingly, it is experimentally known that substitutional cation dopants (e.g., Si,[1] Zr,[11] Y,[12] Al,[13] and La[14]) greatly facilitate the formation of FE hafnia.[15] This suggests that, for a suitably chosen dopant A, the mixture $Hf_{1-x}A_xO_2$ will undergo a paraelectric (PE) to FE transition as x increases, thus displaying a morphotropic phase boundary like many perovskite oxides do. (For example, $Sr_{1-x}Ba_xTiO_3$ undergoes such a transformation for increasing Ba content.[16]) First-principles methods based on the density functional theory (DFT) are ideally suited to reveal such morphotropic transitions; however, as far as we know, the results for doped hafnia have been negative: all DFT studies predict that doping by itself is not sufficient to stabilize the FE polymorph over the PE ground state of the compound.[17–22]

This work originated from our attempts at using doping to improve the electromechanical responses of FE hafnia. In our simulations with representative tetravalent dopants, it quickly became clear that (some) doping atoms have a (very strong) preference to adopt specific spatial arrangements. An important conclusion follows: it is not appropriate to assume—as implicitly done in the all cited DFT works except the study by Falkowski et al.[21] and, to some extent, the study by Künneth et al.[18]—that the dopants locate randomly in the HfO₂ lattice. We thus focus on this issue and address the following questions: What is the preferred spatial configuration of substitutional cation dopants in HfO₂? Can dopant ordering result in a stronger stabilization of the FE phase over the PE polymorphs?

For simplicity, here we consider doping with two tetravalent cations, Si and Zr, that have been extensively studied experimentally. We assume that the isovalent replacement of Hf by Si or Zr occurs without any accompanying defect or charged state. Also, we focus on the lowest energy and most common FE phase of hafnia, which has orthorhombic symmetry $Pca2_1$[23–25], and we denote "FE-o" in the following; thus, we do not consider here other FE polymorphs recently reported.[25,26] HfO₂ has many PE phases, but here we consider only two: the common monoclinic phase, with $P2_1/c$ symmetry and denoted "PE-m" in the following, which is stable at ambient

conditions and constitutes the ground state of the pure compound,[25] and the PE tetragonal polymorph with space group $P4_2/nmc$ and denoted "PE-t" in the following, which has been discussed as a bridge state, leading to the stabilization of the FE-o structure[7,23] and whose relevance in this work will be made clear in the following paragraphs.

Most of our calculations are carried out in a 48-atom supercell containing 16 $Hf_{1-x}A_xO_2$ formula units (**Figure 1** and Supporting Information for details). This supercell allows us to consider composition steps Δx of 0.0625 (6.25%), and we study mixings up to $x = 0.5$ (50%). Whenever we have more than one dopant in the supercell, we study a representative number of spatial arrangements, including distinct limit cases: isolated dopants, clustering forming quasispherical aggregates, dopants forming layers in different cyrstallographic planes, dopants intercalated with the Hf atoms, etc. All in all, we study 4 different

Figure 1. Representative low-energy structures of the $Hf_{1-x}Si_xO_2$ compound, obtained from structural relaxations of the 48-atom supercell mentioned in the text. a) The most stable atomic ordering obtained for the PE-t polymorph at $x = 0.5$; the Hf and Si atoms are intercalated. b) The most stable atomic ordering obtained for the FE-o polymorph at $x = 0.25$; the Si dopants form a layer perpendicular to the c crystallographic axis, which coincides with the direction of FE polarization (marked with an arrow).

orders for 12.5% doping, 12 for 25%, 17 for 31.25%, 16 for 37.5%, 12 for 43.75%, and 12 for 50%. For the DFT simulations, we use standard methods implemented in the VASP package;[27,28] details are shown in the Supporting Information, including some results on the influence of the density functional used in the simulations.

We focus on the calculation of formation energies of the different polymorphs as a function of composition. For a concentration x of dopant A, this quantity is defined as

$$E_{for}(x) = E(x) - (1 - x)E_{HfO_2} - xE_{AO_2} \qquad (1)$$

Here $E(x)$ is the energy of the $Hf_{1-x}A_xO_2$ compound as computed for a particular polymorph and arrangement of the A dopants; further, E_{HfO_2} and E_{AO_2} are the ground-state energies of the pure HfO_2 and AO_2 materials, respectively. The PE-m phase is considered to be the ground state of HfO_2 and ZrO_2.[24,25] For SiO_2, we use the $I\bar{4}2d$ structure reported in the study by Coh and Vanderbilt.[29]

Let us discuss our results following the progress of our simulations and discoveries. Our initial calculations focused on comparing the PE-m and FE-o polymorphs, using the mentioned 48-atom supercell. The corresponding results are shown in **Figure 2** as open red (PE-m) and open blue (FE-o) symbols. We find a marked difference between the behavior of the two dopants. For Si (Figure 2a), the energy differences between different dopant arrangements are massive, with the gaps of as much as 400 meV per formula unit (f.u.), separating the most and least stable configurations. In contrast, the Zr dopants (Figure 2b) present a much weaker tendency toward ordering, with many low-lying dopant arrangements yielding energies within a window of 1 meV f.u.$^{-1}$

It is also worth noting that, for Si doping, formation energies are always positive, implying that $Hf_{1-x}Si_xO_2$ mixtures are metastable. In contrast, the PE-m phase of $Hf_{1-x}Zr_xO_2$ presents negative formation energies, indicating that there is a thermodynamic drive
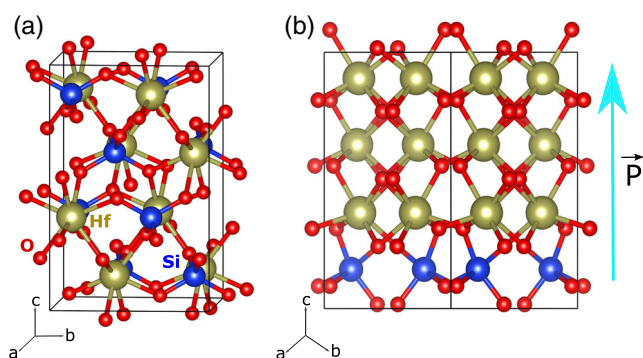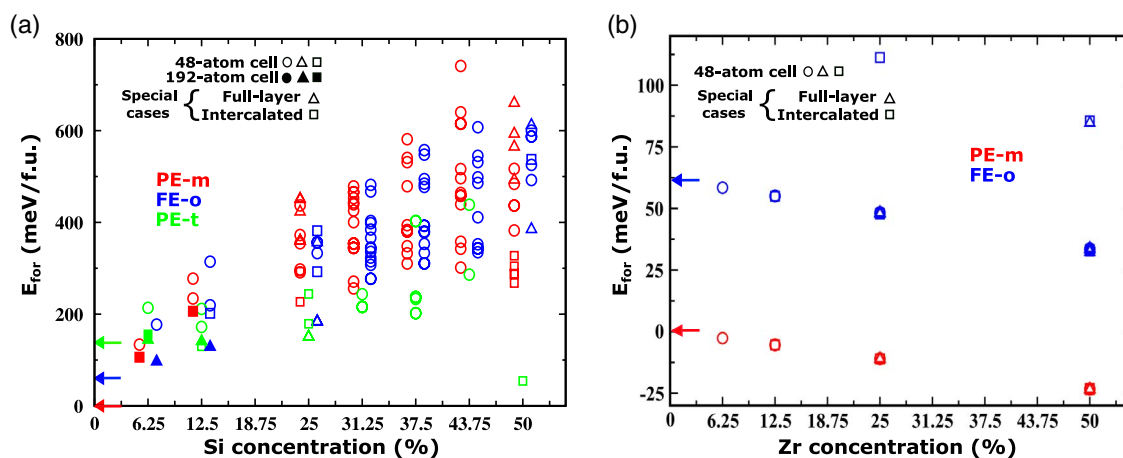

Figure 2. Formation energies E_{for} corresponding to various polymorphs (marked with different colors), dopant compositions, and dopant arrangements. Energies are given in meV per HfO_2-equivalent f.u.; note that the energy scale is not the same in both panels. a) Si doping and b) Zr doping. In (a), at each composition considered, the results for PE-m and FE-o polymorphs are slightly shifted horizontally, for visibility. Squares are used for arrangements where the Hf and dopant atoms are perfectly intercalated, whereas triangles correspond to configurations presenting perfect dopant layers; circles are used for any other dopant order, including defective layering or intercalation. The colored arrows placed at $x = 0$ mark the energies of PE-m (red), FE-o (blue), and PE-t (green, only in (a)) polymorphs as computed for pure HfO_2, taking the PE-m solution as the zero of energy.

toward forming such solid solutions. More interestingly, for Si doping, the PE-m and FE-o structures occupy the same energy range and clearly compete; in contrast, the PE-m state is clearly dominant for all considered Zr compositions. In the following we focus on Si doping, which is clearly more intriguing.

We find that, in some cases, the relaxation of the Si-doped PE-m and FE-o structures yields a different solution, namely, the PE-t polymorph represented with green open symbols in Figure 2a. The PE-t state can be very stable; in particular, the Si-doped structure with the lowest formation energy, which occurs for a Si concentration of 50% and is shown in Figure 1a, has this symmetry. Having found that the PE-t state becomes relevant upon doping, we run for this polymorph all the dopant arrangements previously considered for PE-m and FE-o at 6.25% and 12.5% concentrations. The results, represented by open green symbols in Figure 2a, show that the PE-t state becomes dominant as the amount of Si grows. (A similar stabilization of PE-t has already been reported in the study by Falkowski et al.[21]) Even more interestingly, our results also show that the FE-o polymorph becomes more stable than the PE-m state for Si concentrations of 12.5–25%.

By inspecting the structures of the lowest- and highest-energy dopant arrangements, we can identify the features resulting in more stable configurations. Our findings are shown in **Figure 3**, where Si—O and Hf—O pairs separated by less than 2.4 Å are displayed as forming a chemical bond. Let us start by noting that Si is considerably smaller than Hf. More specifically, the tabulated covalent radii of Hf and Si are 1.87 and 1.11 Å, respectively;[30] as for the ionic radii of Hf^{4+} and Si^{4+}, we have 0.7 and 0.4 Å, respectively.[31] This size difference suggests that, as compared with Hf, the Si dopants will prefer relatively small oxygen coordination numbers, as we indeed observe in our results. More specifically, we find that some of the most stable structures display SiO_4 groups forming nearly regular tetrahedra, as shown in Figure 3a. In particular, the SiO_4 coordination is typical of the doped tetragonal polymorph, and it characterizes the lowest-energy PE-t solutions, including the structure shown in Figure 1a.

A second usual coordination involves SiO_5 groups forming a (distorted) square-base pyramid, as shown in Figure 3b. All Si dopants present this kind of environment in the lowest-lying PE-m and FE-o states, as is the case of the polar structure in Figure 1b. Finally, we also find higher Si coordinations, as, e.g., the quasioctahedral SiO_6 groups shown in Figure 3c, that are typical of high-lying PE-m and FE-o configurations.

Related trends can be identified by paying attention to the environment of the oxygens: without exception, in all our lowest-lying structures, each oxygen is bound to one Si and two Hf atoms, as shown in Figure 3d; in contrast, structures displaying coordination complexes like that of Figure 3e lie at higher energies, and features as those in Figure 3f are typical of even less stable cases. Hence, our results suggest that the lowest-energy states are those whose chemical-bond topology allows the dopants to form the most stable bonding complexes, namely, the ones in Figure 3a,b,d.

Interestingly, a group of low-energy states presents a long-range order whereby the Si dopants are intercalated with the Hf atoms, as in the case of Figure 1a; this order, represented by squares in Figure 2a, is typical of the lowest-lying PE-m structures and some of the most stable PE-t states. In contrast, the remaining low-energy structures are characterized by a layering of the Si dopants; such layered structures, represented by triangles in Figure 2a and shown in Figure 1b, are typical among the lowest-lying FE-o solutions and some of the most stable PE-t states. Nevertheless, as the data in Figure 2a show, intercalation or layering alone does not guarantee that the doped structure will have a low formation energy. Indeed, specific details of the ordering are critical for a low-energy state to occur: most importantly, in the most stable Si-doped FE-o solutions, the dopant layers are perpendicular to the polar c axis (Figure 1b), whereas in the most stable layered PE-t structures, the dopants occupy planes perpendicular to the a crystallographic axis.

One may wonder whether our 48-atom supercell is realistic to investigate the relative stability of these three structures in the limit of small dopings; for example, for a doping concentration
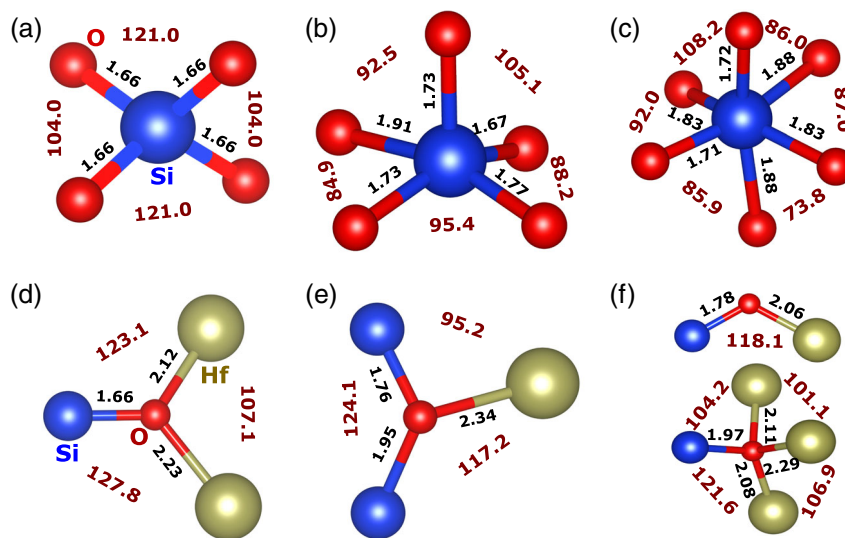

Figure 3. Representative local environments of a–c) Si and d–f) O atoms, as obtained from our simulations (see text). We indicate bond distances (in Å) and bond angles (in degrees).

of 6.25%, the size and shape of this supercell are incompatible with having a complete dopant layer, and only isolated dopants can be studied. Can the peculiar orders observed at higher concentrations, which favor the FE-o and PE-t states, result in the stabilization of such structures for lower doping levels? To test this, we run simulations in elongated 192-atom supercells, as those shown in **Figure 4**, considering the most energetically favorable dopant arrangements previously identified: a localized region with intercalated Hf/Si atoms for PE-m (Figure 4a) and PE-t (Figure 4b) polymorphs, and suitably oriented layers of Si dopants for PE-t (Figure 4c) and FE-o (Figure 4d) structures. The corresponding formation energies are shown as filled symbols in Figure 2a. These results indicate that the FE-o state with full Si layers constitutes the lowest-energy solution at 6.25%, thus predicting that the FE-o phase is the thermodynamically stable ground state of HfO$_2$ upon moderate Si doping! Then, as the Si concentration increases to 12.5%, the FE-o (layered) and PE-t (intercalated) solutions become essentially degenerate, and for higher dopant contents, the PE-t state dominates.
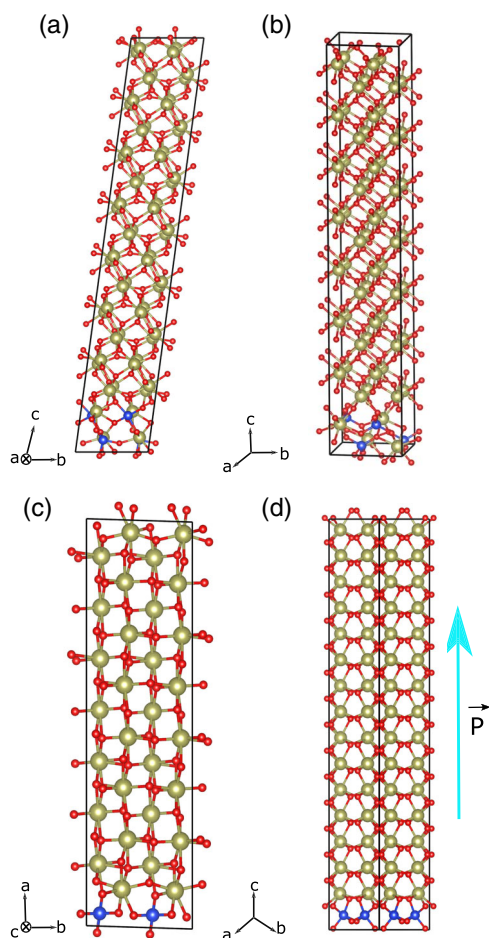
Let us emphasize our results for the 6.25% concentration, as they capture very well the main message of this work. In this case, the open circles in Figure 2a pertain to isolated-impurity calculations as those typically reported in previous DFT studies.[17–20,22] The corresponding formation energies largely reflect the energy differences between the pure HfO$_2$ polymorphs, marked by the colored arrows at $x = 0$ in the figure; hence, the PE-m state prevails. However, when the dopants are allowed to adopt their lowest-energy configuration (filled symbols in the figure), strong energy reductions are obtained for the PE-t and FE-o cases, whereas the energy gain is comparatively small for the PE-m polymorph. This divergent behavior is key to stabilizing the FE-o phase over the PE-m state.

For the FE-o phase of pure HfO$_2$, we calculate a polarization of 55 µC cm^{-2}, in agreement with previous literature.[23,24,32] For the doped structure with a 25% Si concentration (Figure 1b), we obtain 44 µC cm^{-2}. Further, for the 6.25% structure in Figure 4d, we obtain 53 µC cm^{-2}. Hence, we predict that the Si dopants stabilize the FE-o phase without harming its FE polarization.

Our findings seem to be mainly related with the size and preferred oxygen coordination of the relatively small Si dopants and the ability of the FE-o and PE-t polymorphs to better accommodate them. If this interpretation is correct, similar behaviors can be expected for other small dopants. Indeed, we have preliminary first-principles evidence that Ge too stabilizes the FE-o polymorph over the PE-m phase when a full c-oriented layer is formed (i.e., when we have a situation analogous to that of Figure 1b). In contrast, our results for Zr suggest that, for large dopants, ordering is not expected, and doping itself is not enough to revert the relative stability of the PE-m and FE-o phases. (Our preliminary first-principles results indicate that the behavior of Ti, Sn, and Pb dopants is similar.) In conclusion, the ordering mechanism to stabilize FE hafnia is not active for large dopants like Zr; the experimental fact that such dopants do favor ferroelectricity must therefore be caused by other factors.

Our theoretical findings have practical implications worth discussing. Most importantly, they suggest that, by depositing thin SiO$_2$ layers during the growth of hafnia films (so that the silica content adds up to about 6–12% of the material), one should be able to reliably obtain samples in the FE-o phase. The need for a "wake-up" step to observe the FE behavior (as is typical in hafnia thin films[33,34]) would be much reduced in such samples, if present at all, as the FE-o phase is their thermodynamic ground state. The predicted most stable geometry, with polarization lying along the growth (out-of-plane) direction, is all but ideal to maximize the remnant polarization of the films, not favoring any particular polar state and causing no imprint.

This proposed preparation strategy could be realized using techniques that allow great control of epitaxial growth, like, e.g., pulsed laser deposition. Nevertheless, it is important to note that our ideal scenario is strongly reminiscent of how most FE hafnia films are actually grown, via atomic layer deposition (ALD), where the dopant ratio is achieved by performing a dopant oxide ALD cycle after a certain number of HfO$_2$ cycles.[15] ALD-grown films are then subject to thermal treatment to induce crystallization; whereas dopants may diffuse at this step, the resulting samples still present a modulation in dopant concentration along the growth direction, thus displaying diffuse dopant

Figure 4. The 192-atom supercells used to investigate, in the limit of very low dopant concentrations, the relative stability of the most favorable dopant arrangements identified in this work. a) PE-m polymorph with a region of intercalated Hf/Si atoms; b) PE-t polymorph with a region of intercalated Hf/Si atoms; c) PE-t polymorph with an a-oriented dopant layer; and d) FE-o polymorph with a c-oriented dopant layer.

layers.[35,36] Hence, when the ALD samples are subject to the wake-up treatment—i.e., the application of alternate electric fields, typically along the out-of-plane direction—they are (according to our results) suitably preconditioned to yield the FE-o phase. We thus believe the present findings are consistent with the usual experimental route to obtain FE hafnia and partly explain why it works. They also indicate that controlling the layering of small dopants may be key to produce better samples.

Having said this, we should bear in mind that our study is limited to ideal phases of doped HfO_2, the connection with experiment being far from perfect. ALD films are randomly oriented,[37] which implies that, in principle, a good alignment between the dopant layers and specific crystallographic axes (e.g., the polar axis of the FE-o phase) will be possible only in a fraction of the grains. Similarly, the wake-up process is a complex one, known to involve many effects: from transformation of nonpolar regions into polar ones[38] and reorientation of ferroelastic domains[7] to movement of defects[33] and modification of internal bias fields.[39] Hence, it would be naive to take our predictions as a fail-safe strategy to obtain perfect samples of FE hafnia. Yet, they do provide us with a definite motivation to explore directions focused on dopant ordering.

We conclude by noting that, HfO_2 being such a polymorphic material, this study could be extended by considering dopant ordering in other low-lying metastable phases. Further, one could also use advanced DFT methods for structure discovery[40,41] to identify even more stable dopant arrangements. Such investigations might impact the predicted relative stability of doped HfO_2 polymorphs and are worth tackling in the future. Nevertheless, notwithstanding future extensions and improvements, the basic conclusion of this work—namely, that the spatial arrangement of small dopants in HfO_2 is critically important—is clear and robust. Further, its most obvious consequence—that, when accounting for the possible spatial arrangements of the dopants, the formation energies of the dominant polar and nonpolar polymorphs fall within the same range—also seems robust. Hence, the present results should definitely change the way we think of dopants in HfO_2 and how they help stabilize its polar phase.

Supporting Information

Supporting Information is available from the Wiley Online Library or from the author.

Acknowledgements

Conflict of Interest

The authors declare no conflict of interest.

[1] T. S. Böscke, J. Müller, D. Bräuhaus, U. Schröder, U. Böttger, *Appl. Phys. Lett.* **2011**, *99*, 102903.

[2] J. Müller, T. S. Böscke, U. Schröder, S. Mueller, D. Bräuhaus, U. Böttger, L. Frey, T. Mikolajick, *Nano Lett.* **2012**, *12*, 4318.

[3] E. Yurchuk, J. Müller, S. Knebel, J. Sundqvist, A. P. Graham, T. Melde, U. Schröder, T. Mikolajick, *Thin Solid Films* **2013**, *533*, 88.

[4] R. Materlik, C. Künneth, A. Kersch, *J. Appl. Phys.* **2015**, *117*, 134109.

[5] M. H. Park, Y. H. Lee, H. J. Kim, T. Schenk, W. Lee, K. D. Kim, F. P. G. Fengler, T. Mikolajick, U. Schroeder, C. S. Hwang, *Nanoscale* **2017**, *9*, 9973.

[6] C. Künneth, R. Materlik, A. Kersch, *J. Appl. Phys.* **2017**, *121*, 205304.

[7] T. Shimizu, T. Mimura, T. Kiguchi, T. Shiraishi, T. Konno, Y. Katsuya, O. Sakata, H. Funakubo, *Appl. Phys. Lett.* **2018**, *113*, 212901.

[8] E. D. Grimley, T. Schenk, T. Mikolajick, U. Schroeder, J. M. LeBeau, *Adv. Mater. Interfaces* **2018**, *5*, 1701258.

[9] M. H. Park, Y. H. Lee, T. Mikolajick, U. Schroeder, C. S. Hwang, *Adv. Electron. Mater.* **2019**, *5*, 1800522.

[10] S. Liu, B. M. Hanrahan, *Phys. Rev. Mater.* **2019**, *3*, 054404.

[11] J. Müller, T. S. Böscke, D. Bräuhaus, U. Schröder, U. Böttger, J. Sundqvist, P. Kücher, T. Mikolajick, L. Frey, *Appl. Phys. Lett.* **2011**, *99*, 112901.

[12] J. Müller, U. Schröder, T. S. Böscke, I. Müller, U. Böttger, L. Wilde, J. Sundqvist, M. Lemberger, P. Kücher, T. Mikolajick, L. Frey, *J. Appl. Phys.* **2011**, *110*, 114113.

[13] S. Mueller, J. Mueller, A. Singh, S. Riedel, J. Sundqvist, U. Schroeder, T. Mikolajick, *Adv. Funct. Mater.* **2012**, *22*, 2412.

[14] A. G. Chernikova, D. S. Kuzmichev, D. V. Negrov, M. G. Kozodaev, S. N. Polyakov, A. M. Markeev, *Appl. Phys. Lett.* **2016**, *108*, 242905.

[15] M. H. Park, Y. H. Lee, H. J. Kim, Y. J. Kim, T. Moon, K. D. Kim, J. Müller, A. Kersch, U. Schroeder, T. Mikolajick, C. S. Hwang, *Adv. Mater.* **2015**, *27*, 1811.

[16] V. V. Lemanov, E. P. Smirnova, P. P. Syrnikov, E. A. Tarakanov, *Phys. Rev. B* **1996**, *54*, 3151.

[17] R. Batra, T. D. Huan, G. A. Rossetti, R. Ramprasad, *Chem. Mater.* **2017**, *29*, 9102.

[18] C. Künneth, R. Materlik, M. Falkowski, A. Kersch, *ACS Appl. Nano Mater.* **2018**, *1*, 254.

[19] R. Materlik, C. Künneth, T. Mikolajick, A. Kersch, *Appl. Phys. Lett.* **2017**, *111*, 082902.

[20] R. Materlik, C. Künneth, M. Falkowski, T. Mikolajick, A. Kersch, *J. Appl. Phys.* **2018**, *123*, 164101.

[21] M. Falkowski, C. Künneth, R. Materlik, A. Kersch, *NPJ Comput. Mater.* **2018**, *4*, 73.

[22] M. Dogan, N. Gong, T. P. Ma, S. Ismail-Beigi, *Phys. Chem. Chem. Phys.* **2019**, *21*, 12150.

[23] T. D. Huan, V. Sharma, G. A. Rossetti, R. Ramprasad, *Phys. Rev. B* **2014**, *90*, 064111.

[24] S. E. Reyes-Lillo, K. F. Garrity, K. M. Rabe, *Phys. Rev. B* **2014**, *90*, 140103.

[25] S. Barabash, *J. Comput. Electron.* **2017**, *16*, 1227.

[26] Y. Wei, P. Nukala, M. Salverda, S. Matzen, H. J. Zhao, J. Momand, A. S. Everhardt, G. Agnus, G. R. Blake, P. Lecoeur, B. J. Kooi, J. Íñiguez, B. Dkhil, B. Noheda, *Nat. Mater.* **2018**, *17*, 1095.

[27] G. Kresse, J. Furthmüller, *Phys. Rev. B* **1996**, *54*, 11169.

[28] G. Kresse, D. Joubert, *Phys. Rev. B* **1999**, *59*, 1758.

[29] S. Coh, D. Vanderbilt, *Phys. Rev. B* **2008**, *78*, 054117.

[30] B. Cordero, V. Gómez, A. E. Platero-Prats, M. Revés, J. Echeverría, E. Cremades, F. Barragán, S. Alvarez, *Dalton Trans.* **2008**, *21*, 2832.

[31] R. D. Shannon, *Acta Crystallogr. Sect. A* **1976**, *32*, 751.

[32] S. Clima, D. J. Wouters, C. Adelmann, T. Schenk, U. Schroeder, M. Jurczak, G. Pourtois, *Appl. Phys. Lett.* **2014**, *104*, 092906.

[33] D. Zhou, J. Xu, Q. Li, Y. Guan, F. Cao, X. Dong, J. Müller, T. Schenk, U. Schröder, *Appl. Phys. Lett.* **2013**, *103*, 192904.

[34] T. Schenk, U. Schroeder, M. Pešić, M. Popovici, Y. V. Pershin, T. Mikolajick, *ACS Appl. Mater. Interfaces* **2014**, *6*, 19744.

[35] P. D. Lomenzo, Q. Takmeel, C. Zhou, C. C. Chung, S. Moghaddam, J. L. Jones, T. Nishida, *Appl. Phys. Lett.* **2015**, *107*, 242903.

[36] C. Richter, T. Schenk, M. H. Park, F. A. Tscharntke, E. D. Grimley, J. M. LeBeau, C. Zhou, C. M. Fancher, J. L. Jones, T. Mikolajick, U. Schroeder, *Adv. Electron. Mater.* **2017**, *3*, 1700131.

[37] T. Schenk, C. M. Fancher, M. H. Park, C. Richter, C. Künneth, A. Kersch, J. L. Jones, T. Mikolajick, U. Schroeder, *Adv. Electron. Mater.* **2019**, *5*, 1900303.

[38] E. D. Grimley, T. Schenk, X. Sang, M. Pešić, U. Schroeder, T. Mikolajick, J. M. LeBeau, *Adv. Electron. Mater.* **2016**, *2*, 1600173.

[39] T. Schenk, M. Hoffmann, J. Ocker, M. Pešić, T. Mikolajick, U. Schroeder, *ACS Appl. Mater. Interfaces* **2015**, *7*, 20224.

[40] *Modern Methods of Crystal Structure Prediction* (Ed: A. R. Oganov), Wiley-VCH, Weinheim, Germany **2010**.

[41] Y. Wang, J. Lv, L. Zhu, Y. Ma, *Comput. Phys. Commun.* **2012**, *183*, 2063.

2000047 (6 of 6)